Fusion of FDG and FMZ PET Reduces False Positive in Predicting Epileptogenic Zone

Bingyang Cai[#], Shize Jiang[#], Hui Huang, Jiwei Li, Siyu Yuan, Ya Cui, Weiqi Bao, Jie Hu, Jie Luo[*], Liang Chen[*]

ABSTRACT

BACKGROUND AND PURPOSE: Epilepsy, a globally prevalent neurological disorder, necessitates precise identification of the epileptogenic zone (EZ) for effective surgical management. While the individual utilities of FDG PET and FMZ PET have been demonstrated, their combined efficacy in localizing the epileptogenic zone remains underexplored. We aim to improve the non-invasive prediction of epileptogenic zone (EZ) in temporal lobe epilepsy (TLE) by combining FDG PET and FMZ PET with statistical feature extraction and machine learning.

MATERIALS AND METHODS: This study included 20 drug-resistant unilateral TLE patients (14 mesial TLE, 6 lateral TLE), and two control groups (N=29 for FDG, N=20 for FMZ). EZ of each patient was confirmed by post-surgical pathology, and one-year follow-up, while propagation zone (PZ) and non-involved zone (NIZ) were derived from the epileptogenicity index based on presurgical stereo-encephalography (SEEG) monitoring. Whole brain PET scans were obtained with dual tracers [^{18}F]FDG and [^{18}F]FMZ on separate days, from which standard uptake value ratio (SUVR) was calculated by global mean scaling. Low-order statistical parameters of SUVRs and t-maps derived against control groups were extracted. Additionally, fused FDG and FMZ features were created using arithmetic operations. Spearman correlation was used to investigate the associations between FDG and FMZ, while multiple linear regression analysis was used to explore the interaction effects of imaging features in predicting epileptogenicity. Crafted imaging features were used to train logistic regression models to predict EZ, whose performance was evaluated using 10-fold cross-validation at ROI-level, and leave-one-patient-out cross-validation at patient-level.

RESULTS: FDG SUVR significantly decreased in EZ and PZ compared to NIZ, while FMZ SUVR in EZ significantly differed from PZ. Interaction effects were found between FDG and FMZ in their prediction of epileptogenicity. Fusion of FDG and FMZ provided the best prediction model with an area under the curve (AUC) of 0.86 [0.84-0.87] for EZ vs. NIZ and an AUC of 0.79 [0.77-0.81] for EZ vs. PZ, eliminating 100% false positives in 50% of patients, and ≥80% FPs in 90% patients at patient level.

CONCLUSIONS: Combined FDG and FMZ offer a promising avenue for non-invasive localization of the epileptogenic zone in TLE, potentially refining surgical planning.

ABBREVIATIONS: AUC = Area under the curve; EI = Epileptogenicity index; EZ = Epileptogenic zone; FMZ = Flumazenil; $GABA_A$ = Gamma-aminobutyric acid type A; NIZ = Non-involved zone; PZ = Propagation zone; SEEG = Stereo-electroencephalography; SUVR = Standard uptake value ratio; TLE = Temporal lobe epilepsy.

Received month day, year; accepted after revision month day, year.
From the School of Biomedical Engineering (B.C., H.H., J.L., S.Y., Y.C., J.L.), Shanghai Jiao Tong University, Shanghai, China; Department of Neurosurgery (S.J., J.H., L.C.), and PET Center (W.B.), Huashan Hospital, Fudan University, Shanghai, China

[#]Bingyang Cai and Shize Jiang contributed equally to this work. *Liang Chen and Jie Luo are co-corresponding authors.
This work was supported by the National Natural Science Foundation of China (No.82272116, No.62101321) and the Science and Technology Commission of Shanghai municipality frontier innovation program (No.24DP3200600). The authors declare no conflicts of interest related to the content of this article.

Please address correspondence to Jie Luo, PhD, School of Biomedical Engineering, Shanghai Jiao Tong University, 1954 Huashan Road, Shanghai, 200030 China; jieluo@sjtu.edu.cn.

SUMMARY SECTION

PREVIOUS LITERATURE: Invasive stereo-electroencephalography (SEEG) is currently used to capture epileptogenic networks and to identify epileptogenic zones (EZ) for drug-resistant epilepsy patients. [^{18}F]FDG PET is widely used to identify hypometabolic regions in the epileptic brain, which has been shown to correlate with SEEG-defined EZ; [^{18}F]FMZ PET targets benzodiazepine sites on $GABA_A$ receptors, providing insights into inhibitory neurotransmission changes in epilepsy, yet no report had associated FMZ uptake with SEEG-defined epileptogenic networks. A meta-analysis of 34 [^{18}F]FDG studies, 3 [^{11}C]FMZ studies, and 7 combined studies reported comparable lesion detection performances. However, whether image fusion of FDG and FMZ enhances EZ prediction remains unexplored.

KEY FINDINGS: [^{18}F]FDG and [^{18}F]FMZ uptake exhibit significant decreases in EZ, while showing an interaction effect in predicting epileptogenicity. Their image fusion features effectively distinguish EZ from propagation and non-involved zones, achieving an 80% true-positive rate for EZ prediction and reducing false positives by ≥80% in 90% of patients.

KNOWLEDGE ADVANCEMENT: This study pioneers in characterizing FMZ uptake in SEEG-defined epileptogenic networks, uncovering the interaction effect between FDG and FMZ in the epileptic brain. Fusion of FDG and FMZ shows potential to reduce false positives and enhance accuracy in non-invasive prediction of EZ, offering to enhance diagnostic precision and guide interventions.

INTRODUCTION

Epilepsy, affecting around 50 million people worldwide, is characterized by recurrent spontaneous seizures[1]. Approximately 30% of cases are drug-resistant, often require surgical resection[2]. Accurate localization of the epileptogenic zone (EZ) is crucial. The epileptogenicity index (EI), derived from Stereo-electroencephalography (SEEG) signals, can be used to classify brain regions as EZ, propagation zone (PZ), or non-involved zone (NIZ)[3]. However, SEEG is costly, samples the brain sparsely, and poses surgical risks[4].

[^{18}F]Fluorodeoxyglucose (FDG) PET non-invasively detects metabolic changes and is frequently utilized when MRI exams are inconclusive[5,6]. Reduced glucose uptake may be attributable to neuronal damage, cumulative mitochondrial stress, or enhanced glycogen storage caused by recurrent seizures[7]. Interictal hypometabolism enhances detection sensitivity in MRI-negative temporal lobe epilepsy (TLE)[8,9] and focal cortical dysplasia (FCD) cases[10]. FDG uptake has been reported to decrease in both SEEG-defined EZ and PZ in FCD patients[11].

Flumazenil (FMZ)-based PET, such as [^{11}C]FMZ and [^{18}F]FMZ, target γ-aminobutyric acid receptor A ($GABA_A$) receptors, have also been reported to aid the detection of seizure onset zone for drug-resistant TLE, even in MR-negative cases[6,12,13]. $GABA_A$ receptor-mediated inhibition is a key pathophysiologic mechanism driving increased neuronal excitability and leading to epileptogenesis[14-17]. To date, there is no report on FMZ uptake changes in SEEG-defined epileptogenic networks.

A meta-analysis pooling 34 [^{18}F]FDG studies, 3 [^{11}C]FMZ studies, and 7 [^{11}C]FMZ/[^{18}F]FDG studies reported comparable lesion detection performances of FDG PET and FMZ PET[18]. Previous studies have demonstrated that reading both FMZ PET and FDG PET scans can assist in EZ localization during clinical pre-surgical evaluations[13,19,20]. This study hypothesizes that image feature fusion of FDG and FMZ could enhance epileptogenic zone localization accuracy, given their separate pathophysiological mechanisms. We assessed the performance of FDG and FMZ, both separately and combined, in classifying EZ in TLE patients using machine learning. We also explored interactions between FDG and FMZ changes to understand their synergy in localizing the EZ. Methods and results adhere to the STARD guidelines (Online Supplemental Data).

MATERIALS AND METHODS

Patient Recruitment

This retrospective study was approved by the Institutional Review Board of Huashan Hospital (IRB No. KY2015-256), and informed consent was obtained from all participants who were drug-resistant TLE patients being considered for presurgical evaluations between 2018 and 2022. Participants underwent both FDG and FMZ PET scans for clinical evaluations. Within this cohort, twenty subjects (male/female 11/9, aged 8-46) with SEEG recordings of 2-3 seizures and their EZ location confirmed by post-surgical outcomes and follow-up (Figure 1A).

Three control groups were included for comparison: healthy volunteers for [^{18}F]FDG PET scans (IRB No. KY2021-454), structural MRI data from the Human Connectome Project's (HCP) 1200 subjects data release (*https://www.humanconnectome.org/study/hcp-young-adult/document/1200-subjects-data-release*), and age-matched drug-resistant epilepsy patients who were scanned for presurgical evaluation with negative MRI and negative FMZ PET were selected as the FMZ control group. This choice was primarily constrained by ethical considerations, preventing the recruitment of healthy volunteers for FMZ PET.

SEEG Recordings

Video-SEEG monitoring employed intracerebral multi-contact electrodes, with 8-16 contacts (2 mm length, 0.8 mm diameter, 1.5 mm spacing). The iEEGview toolbox[21] located each contact anatomically, assigning brain regions of interest (ROIs) per the Destrieux atlas[22]. Electrodes in white matter were excluded due to signal interpretation challenges[23]. Bipolar re-referencing minimized common reference and volume conduction effects[24].

The epileptogenic zone was defined by calculating the Epileptogenicity Index (EI) at each contact, based on high-frequency energy ratios relative to seizure onset time[3]. The channel with the highest EI was selected for regions with multiple channels. Brain areas with $EI > 0.3$ were classified as EZ; those with $EI \leq 0.3$ and sustained seizure discharge as PZ; all others as NIZ[3].

Image Acquisition

All PET imaging was performed on a Siemens Biograph mCT Flow Edge 128 scanner. [^{18}F]FDG PET scans were conducted 50 minutes after injecting ~296MBq (8mCi) of [^{18}F]FDG, lasting 10 minutes. Images were reconstructed with time-of-flight and TrueX algorithm (4 iterations, 21 subsets), smoothed with a 3.5 mm Gaussian kernel, and attenuation-corrected with hybrid CT images. The reconstruction matrix was 256×256×148 with a resolution of 2mm×2mm×1.5mm.

In a separate session, [^{18}F]FMZ PET scans were acquired (Online Supplemental Data). [^{18}F]Flumazenil was synthesized via standard nucleophilic radiofluorination of the corresponding nitro-analog precursor with K^{18}F/kryptofix complex in DMF at 160°C for 30 minutes[25], then purified by high-performance liquid chromatography and sterilized. Scanning began 20 minutes after injecting ~370MBq (10mCi) of [^{18}F]FMZ, lasting 20 minutes, with reconstruction settings consistent with the FDG session.

MRI structural images were obtained using a 3D Gradient-Echo BRAin VOlume (BRAVO) sequence with a resolution = 0.9×0.9×1.0 mm^3, TR/TE/TI = 8.2/3.2/450 ms, FOV = 240×240×200 mm^3, and a 2D T2-weighted FLAIR sequence in three orthogonal directions with a resolution = 0.9×0.9 mm^2, slice thickness = 3 mm, TR/TE/TI = 8490/90/2438 ms, FOV = 210×300 mm^2, 46 slices (Online Supplemental Data).

Data Processing and Feature Extraction

MRI structural images were parcellated using Freesurfer with Destrieux atlas, yielding 148 cortical and 14 subcortical ROIs[22]. ROI volumes were calculated after intracranial volume correction and normalized to z-scores using ComBat-adjusted HCP healthy controls[26]. Standard uptake value ratio (SUVR) maps of PET images were obtained via global mean scaling. Individual t-maps were calculated using statistical parametric mapping (SPM) in Montreal Neurological Institute (MNI) space, then transformed into individual T1 space (Figure 1B).

Low-order statistical parameters[27] (mean, median, maximum, minimum, range, standard deviation, variance, root mean square (RMS), mean absolute deviation (MAD), uniformity, skewness, energy, entropy, kurtosis, totaling 14 features) were extracted for each ROI from SUVR maps and t-maps for both FDG and FMZ. SUVR features were further normalized as z-scores based on control groups.

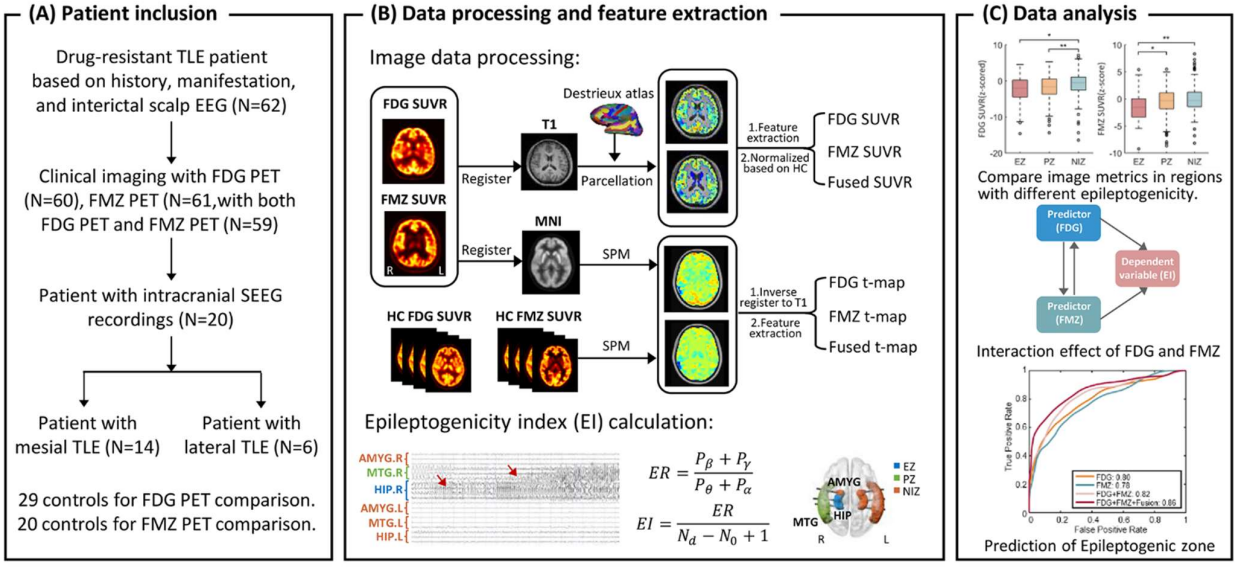

FIG 1. Workflow of data collection and processing. (A) Flow chart of patient inclusion. (B) Workflow of data processing and feature extraction. The SUVR maps of FDG and FMZ images are registered to T1-weighted space and parcellate into 162 ROIs. Individual t-maps of each patient compared to healthy subjects are calculated using statistical parametric mapping in MNI space and then transformed into individual T1 space. Low-order statistical parameters and fused molecular features are extracted for each ROI from both SUVR maps and t-maps for FDG and FMZ. The epileptogenicity index of the SEEG signals is calculated, with regions subsequently labeled as EZ, PZ, and NIZ based on their epileptogenicity. (C) The Mann-Whitney U test and the interaction effect analysis are employed to FDG and FMZ SUVR levels across brain regions with different epileptogenicity. Finally, the extracted molecular features are used to build logistic regression for EZ prediction. AMYG, amygdala; EZ, epileptogenic zone; HIP, hippocampus; L, left; MTG, middle temporal gyrus; NIZ, non-involved zone; PZ, propagation zone; R, right; SUVR, standard uptake value ratio; SPM, statistical parametric mapping.

Feature Fusion

Fused imaging features were engineered through arithmetic operations between FDG and FMZ SUVR features (Addition-s, Subtraction-s, Product-s, and Logarithm-s, which is the product of logarithms) and their corresponding t-map features (Addition-t, Subtraction-t, Product-t, and Logarithm-t). Additionally, to account for associations between FDG and FMZ, linear fitting parameters between their t-maps, Slope-t and Intercept-t, were included. This resulted in a total of 10 fusion features.

In this study, 'fused' specifically refers to fusion features, while 'concatenated' describes putting different feature vectors side-by-side to form a new feature vector.

Statistical Analysis

Gender was compared using the chi-square test, while age was compared with the Mann-Whitney U test. To confirm molecular changes in hippocampal sclerosis, the Wilcoxon rank-sum test was used to compare FDG and FMZ SUVR between the ipsilateral and contralateral hippocampi. To evaluate molecular differences among EZ, PZ, and NIZ, we performed analyses using a linear mixed-effects model to capture group-level differences while controlling for random effects across individuals. Group differences between EZ-PZ, EZ-NIZ, and PZ-NIZ were further examined using Mann-Whitney U tests with effect size calculations. Bonferroni-Holm corrections were applied for multiple comparisons. Additionally, to understand whether FDG and FMZ are correlated in the epileptogenic zone, their correlations in regions of varying epileptogenicity were analyzed using Spearman correlation. Statistical significance was set at $p < 0.05$.

Interaction Analysis

Interaction effects between FDG and FMZ in predicting tissue epileptogenicity were examined through a multiple linear regression model[28]. Predictors included FDG, FMZ, and their interaction term (FDG×FMZ). Both variables were mean-centered before analysis[29]. A bias-corrected bootstrap approach (5000 iterations) in IBM SPSS Statistics tested the significance of interaction effects.

Epileptogenic Zone Classification

To evaluate whether combining FDG and FMZ imaging could enhance EZ localization, we employed machine learning methods, specifically the Least Absolute Shrinkage and Selection Operator (LASSO) and logistic regression. The LASSO algorithm was first implemented for feature selection by adding a penalty to the least-squares function to reduce redundancy[30] and enhance predictive power for EI, using 10-fold cross-validation. Logistic regression models then evaluated the capabilities of different modalities in binary classifications of EZ vs. PZ, EZ vs. NIZ, and PZ vs. NIZ with the selected features at both ROI and patient levels. ROI-level classifications used a 10-fold cross-validation and 1,000 random trials to minimize random chance. We evaluated the classification efficacy of different logistic regression models that incorporated single modality features, concatenated features, and concatenated features together with fused imaging features as input. Performance metrics included accuracy, sensitivity, specificity, and the area under the curve (AUC) of receiver operating characteristic (ROC) curves. The Youden index determined optimal cut-off points, and DeLong's test compared AUCs across models. Performance was further observed for mesial and lateral TLE groups using the same model.

At the patient-level, the EZ was classified using leave-one-patient-out cross-validation. A prediction was considered a true positive (TP) if the model detected a brain region labeled as EZ that was included in the surgical resection area. The false positive (FP) rate was calculated by combining the results of EZ vs. PZ and EZ vs. NIZ to find the percentage of contacts falsely assigned as EZ per patient. Patient-level TP and FP were enumerated respectively for mesial and lateral TLE subgroups.

RESULTS

Patient Demographics

Patient demographics and clinical information are provided in Table 1 (Online Supplemental Data), including 14 mesial TLE and 6 lateral TLE. All underwent SEEG and 1-year post-surgery follow-up. Among them, 14 had inconclusive MRI, with 11 bilateral MRI abnormalities and 3 MRI invisible. Patients were compared to healthy controls for FDG PET (sex, $P = 0.99$; age, $P = 0.08$) and the FMZ control group for FMZ (sex, $P = 0.75$; age, $P = 0.12$). Structural comparisons were also made with healthy HCP subjects (sex, $P = 0.40$; age, $P = 0.12$).

Table 1 Patient demographics

Parameter	TLE	HC1	HC2	HCP
Number of subjects	20	29	20	1113
Sex (male/female)	11/9	16/13	10/10	507/606
Age at evaluation (year), median (range)	32(8-46)	37.5(11-52)	25(20-40)	28(22-36)
Age at seizure onset (year), median (range)	16.5(4-40)			
Mesial/lateral TLE	14/6			
Epilepsy duration (year), median (range)	9.5(2-30)			
Seizure frequency (per year), median (range)	30(1-1277)			
Number of patients with SEEG evaluations	20			
Postsurgical outcome Engel Class (I/II-IV)	19/1			

Note: HC1, healthy control group for FDG comparison; HC2, control group for FMZ comparison; HCP, Human Connectome Project

FMZ and FDG PET Show Concordant Findings in Temporal Lobe Epilepsy

In a representative mesial TLE case, FDG SUVR showed hypometabolism in the right hippocampus, while FMZ SUVR displayed decreased Benzodiazepine-$GABA_A$ receptor binding in the same region (Figure 2A), consistent with FLAIR images. Subgroup comparisons revealed significant differences between the ipsilateral vs. contralateral hippocampus in the mesial TLE group ($P = 0.003$ for FDG and $P = 0.01$ for FMZ) (Online Supplemental Data). In a lateral TLE, an MRI-positive patient showed reduced FDG and FMZ SUVR in the right inferior temporal gyrus (Figure 2B). However, the lateral TLE group did not exhibit significant differences in the ipsilateral hippocampus ($P = 0.16$ for FDG and $P = 0.96$ for FMZ) (Online Supplemental Data).

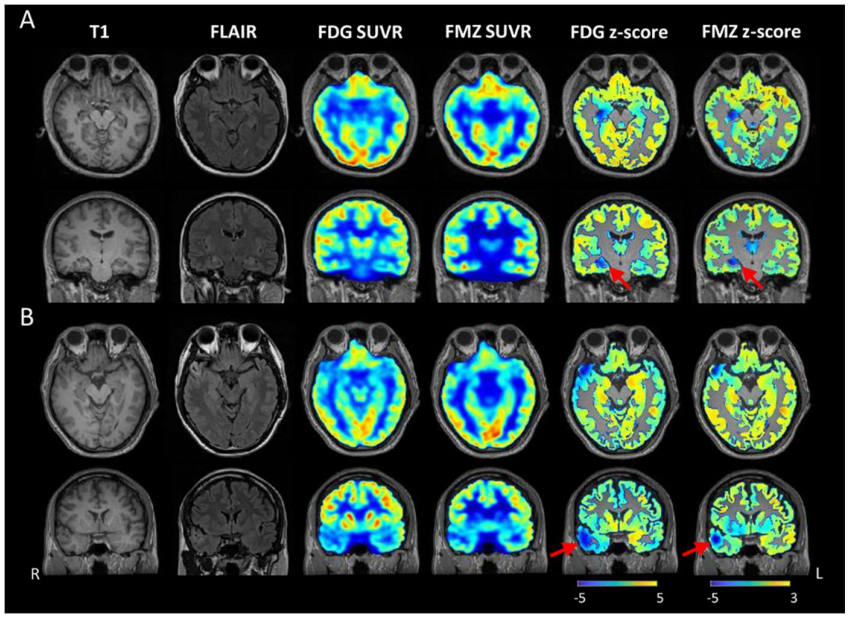

FIG 2. Images of FDG PET and FMZ PET in representative cases. (A) Axial and coronal views of a patient diagnosed with mesial TLE and pathologically confirmed hippocampal sclerosis (patient #7), with T1-weighted image, FLAIR, [^{18}F]FDG PET, [^{18}F]FMZ PET, and corresponding z-scored maps of FDG and FMZ PET from left to right. (B) Axial and coronal views of a patient with lateral TLE in the right inferior temporal gyrus (patient #17).

Relationships Between FMZ, FDG Uptake and Epileptogenicity

The epileptogenicity index derived from SEEG classified brain regions into epileptogenic zone, propagation zone, and non-involved zone. Both FDG and FMZ demonstrated differences among EZ, PZ and NIZ in the linear mixed-effects model ($P < 0.001$ for FDG and $P < 0.001$ for FMZ). Both z-scored FDG and FMZ uptakes significantly decrease in EZ compared to NIZ ($P = 0.002$, Cohen's d = 0.49; $P < 0.001$, Cohen's d = 0.54). FDG SUVR was decreased in PZ compared to NIZ ($P < 0.001$, Cohen's d = 0.34), while FMZ SUVR decreased in EZ compared to PZ ($P = 0.002$, Cohen's d = 0.41) (Figure 3A). The significance threshold was $\alpha < 0.008$ (0.05/6) after correction for multiple comparisons. Gray matter volume shows a decreasing tendency in EZ compared to NIZ, though not significant after corrections ($\alpha < 0.017$ (0.05/3), Online Supplementary Data). FDG and FMZ exhibit stronger positive correlations in EZ than in PZ and NIZ (Figure 3B). These trends were consistent in mesial TLE but not in lateral TLE (Online Supplemental Data). A significant positive correlation between FDG and FMZ was observed in the EZ of each patient (Figure 3C), indicating an association between glucose uptake and $GABA_A$ receptor distribution changes within the epileptogenic zone.

Interaction Effects Between FDG and FMZ

A two-level multiple linear regression tested the interaction effects between FDG and FMZ in predicting EI. Formula (1) estimates the independent contributions of FDG and FMZ, while formula (2) incorporates an interaction term, 'FDG×FMZ'. The analysis showed that FDG and FMZ SUVR independently predicted EI ($P < 0.001$) with predictive power significantly enhanced by the interaction term ($\Delta R^2 = 0.03$, $P = 0.002$). When FMZ is used as a conditional value, the negative association between FDG uptake and EI was strong ($\beta = -0.19$, $P < 0.001$) at low FMZ (1 SD below the mean), but not significant at medium or high FMZ levels ($\beta = -0.09$, $P = 0.08$, at mean FMZ; $\beta = 0.02$, $P = 0.81$, 1 SD above the mean). Similarly, the negative association between FMZ and EI was strongest at low FDG ($\beta = -0.35$, $P < 0.001$), moderate at medium FDG ($\beta = -0.25$, $P < 0.001$), and weakest at high FDG ($\beta = -0.15$, $P = 0.03$) (Figure 3D).

$$\mathrm{EI} = -0.119\mathrm{FDG} - 0.295\mathrm{FMZ} \quad (1)$$

$$\mathrm{EI} = -0.051 - 0.087\mathrm{FDG} - 0.250\mathrm{FMZ} + 0.103\mathrm{FDG} \times \mathrm{FMZ} \quad (2)$$

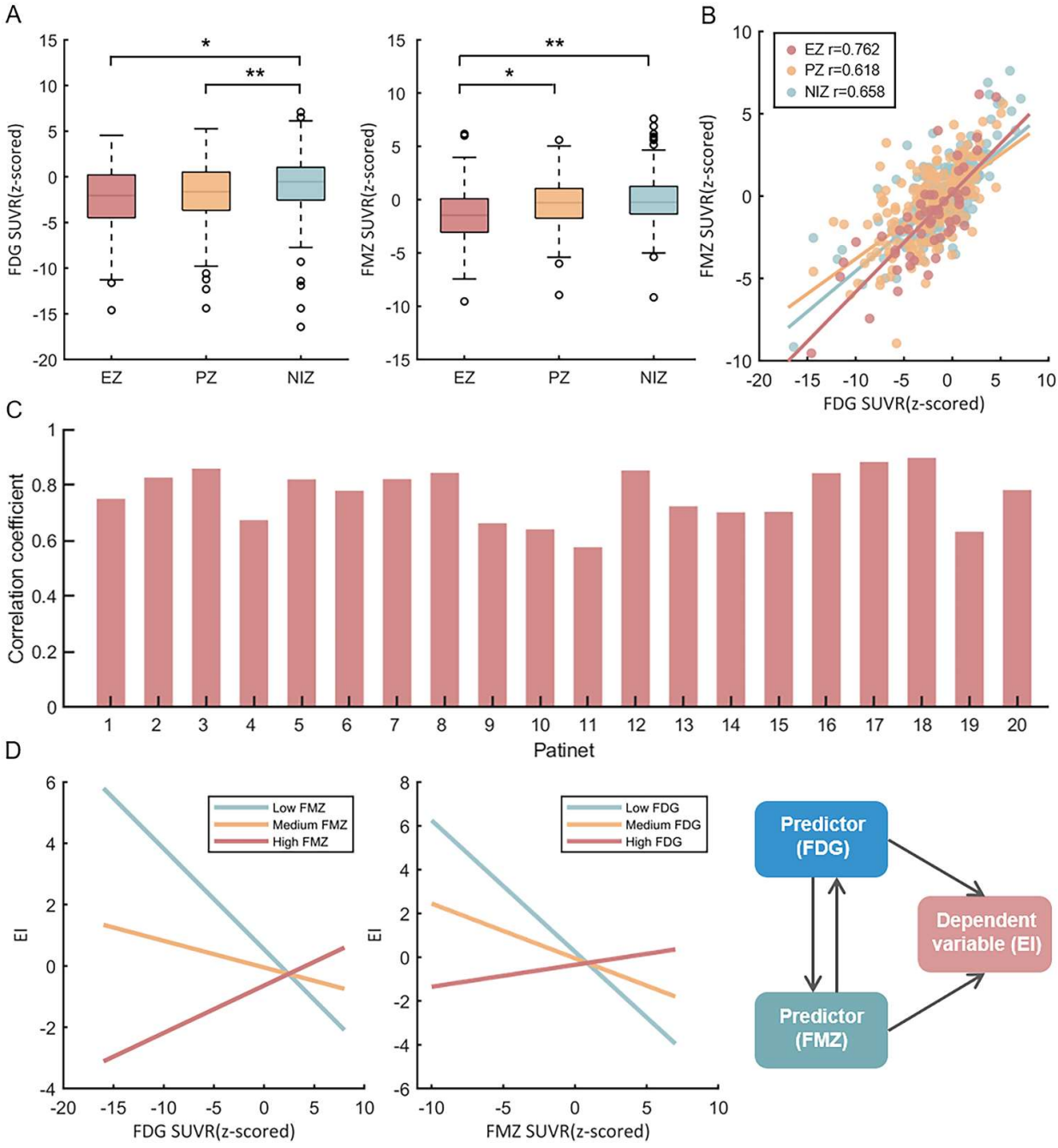

FIG 3. The relationship of FDG and FMZ SUVR among brain regions with different epileptogenicity. (A) Boxplot of z-scored FDG SUVR (left) and boxplot of z-scored FMZ SUVR (right) in regions with different epileptogenicity noted as EZ, PZ, and NIZ. (B) The scatter plot of FMZ vs. FDG shows their associations change with epileptogenicity. (C) Correlation coefficients of FMZ and FDG in EZ of all patients. (D) Interaction effects between FDG and FMZ in predicting epileptogenicity. The relationship between FDG SUVR and EI at three FMZ levels (left). The relationship between FMZ SUVR and EI at three FDG levels (middle). Schematic of the interaction model between FDG and FMZ for EI prediction (right). *P < .05, **P < .01, Mann-Whitney U test under Bonferroni-Holm correction.

Fused FMZ and FDG Provide Improved Prediction of Epileptogenic Zone

Features were ranked by their LASSO regression coefficient (Figure 4A) with the fusion feature "addition of FMZ and FDG t-maps" showing the highest contribution. For EZ vs. NIZ classifications, FMZ performed comparably to FDG (AUC = 0.78 [0.76-0.79], vs. AUC = 0.80 [0.78-0.81]). Their concatenation slightly improved performance (AUC = 0.82 [0.81-0.84]), with fusion features achieving the best results (AUC = 0.86 [0.84-0.87]) (Figure 4B, C). DeLong's test indicates that fusion features significantly outperformed single-modality inputs (P = 0.04 for FDG, P = 0.008 for FMZ). EZ vs. PZ classifications were more challenging, with PZ vs. NIZ separation proving the most difficult (AUC < 0.60). Models predicted EZ more accurately in mesial TLE than in lateral TLE (Online Supplemental Data).

In patient-level EZ prediction, the concatenated FDG, FMZ and fusion model showed a similar detection rate as FDG alone in 80% of

patients (16/20) (Figure 5A), while eliminating all FPs in 50% of patients and ≥80% of FPs in 90% (18/20) of patients (Figure 5B). Both mesial and lateral TLE subtypes showed similar FP performance, but mesial TLE had a higher true positive rate compared to lateral TLE (Figure 5A, C).

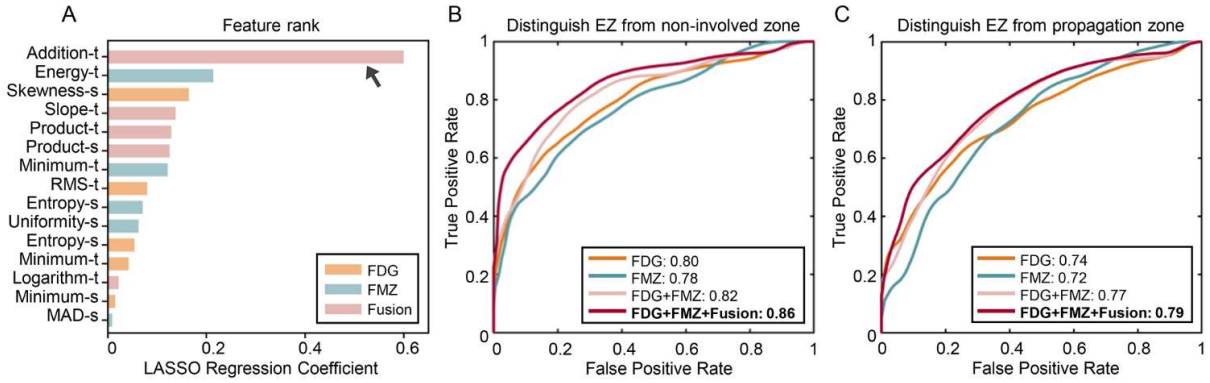

FIG 4. Classification of the epileptogenic zone (EZ) using single or concatenated molecular features at the ROI level. (A) Bar plot showing feature ranking based on LASSO regression coefficients for selected features. The arrow highlights the feature with the highest contribution, 'the addition of FMZ and FDG t-maps', in the LASSO regression model. (B) ROC curves of classification models that distinguish EZ from non-involved zone (NIZ) and (C) ROC curves of classification models that distinguish EZ from propagation zone (PZ) with four different feature inputs. The suffix '-t' means t-map features, while '-s' means SUVR features. RMS, root mean square. MAD, mean absolute deviation.

A

Feature	Number of patients with true positive(%)		
	All subtype (N=20)	Mesial TLE (N=14)	Lateral TLE (N=6)
FDG	16(80)	13(93)	3(50)
FMZ	14(70)	12(86)	2(33)
FDG+FMZ+Fusion	**16(80)**	**13(93)**	**3(50)**

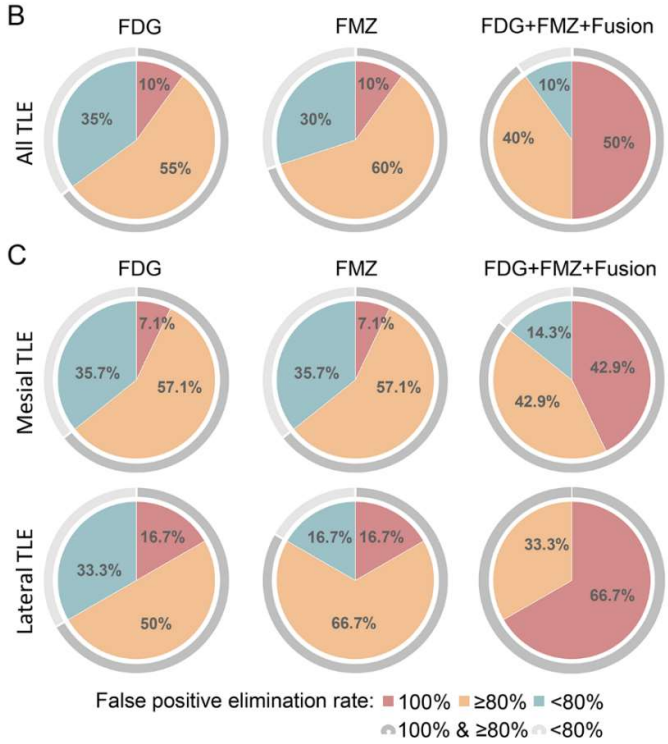

FIG 5. Model performance using single or concatenated molecular features at the patient level. (A) The number of patients with true positive EZ prediction across all subtypes using FDG (a PET tracer for hypometabolism), FMZ (a PET tracer for $GABA_A$ receptor binding), and their fusion feature as inputs. (B) The patient-level false positive rate in all subtypes. (C) The patient-level false positive rate in mesial TLE (above) and lateral TLE (below). Different colors represent the range of false positive elimination: red

indicates 100% elimination; orange represents more than 80% elimination; cyan denotes less than 80% elimination; dark gray indicates the combination of 100% and more than 80% elimination; light gray represents less than 80% elimination.

DISCUSSION

This study demonstrates that [^{18}F]FMZ PET complements the more commonly used [^{18}F]FDG PET in the localization of the epileptogenic zone, reducing false positives. Significant decreases in both FDG and FMZ uptakes were observed in pathologically confirmed lesions. Multi-regression analysis reveals that FDG SUVR interacts with FMZ SUVR in predicting epileptogenicity, with their fused feature contributing the most in classification models.

Interplays Between Glucose Uptake and GABA$_A$ Receptor Availability

FDG and FMZ SUVR exhibited strong positive correlations in EZ of each patient, and weaker correlations in regions with lower epileptogenicity. Previous studies comparing FMZ PET and FDG PET primarily focused on lesion detection[12], rather than their associations. In temporal lobe epilepsy, reduced glucose metabolism may impair GABA$_A$ receptor phosphorylation, affecting GABAergic inhibition[31]. In Huntington's disease, glucose hypometabolism has been shown to precede GABAergic dysfunction[32]. Conversely, dysfunctional GABA$_A$ receptors may elevate neuronal activity, altering glucose metabolism by increasing energy demands[33]. GABAergic neuronal loss would result in decreased glucose uptake and GABA$_A$ receptor availability[34]. Our analysis reveals for the first time that FMZ SUVR interacts with FDG SUVR in predicting epileptogenicity, indicating their fusion may enhance EZ prediction.

Feature Contributions to EZ Classification Models

Machine learning evaluations support synergistic effects between FDG and FMZ. The fused FDG and FMZ feature ranked highest in feature importance, consistent with the interaction effect analysis. In patient-level classification, the dramatic elimination of false positives using fused molecular feature input may be explained by a lack of concurrent hypometabolism and GABA$_A$ down-regulation in regions with transient functional changes.

Model comparisons revealed better performance for mesial than lateral TLE groups at both ROI-level and patient-level (Online Supplemental Data, Figure 5A), which may be attributed to the heterogeneous expression of GABA$_A$ receptor subunits and variations in lesion locations.

Limitations

First, the EZ defined by the epileptogenicity index differs conceptually from the seizure onset zone confirmed by post-surgical seizure freedom. Therefore, for patient-level true positive detection, we used only the EZ that corroborated the seizure onset zone for each patient. The advantage of using EI is that it provides additional insight into the epileptogenic network, including propagation and non-involved zones.

Second, due to challenges in recruiting healthy volunteers for FMZ PET, and inherent bias between our data and the [^{11}C]FMZ brain template (N=16)[35] (e.g. demographic and tracer differences), we formed an FMZ control group comprised of radiologically "normal" epilepsy patients.

Additionally, the small sample size may introduce random variability and bias in machine learning validation, affecting model performance and leading to overfitting. It may also result in an unreliable representation of subgroups, such as lateral versus mesial TLE, potentially skewing results.

Finally, while this study offers valuable insights into the synergistic effects of FDG and FMZ in predicting epileptogenicity, future research should incorporate additional imaging modalities, such as high-resolution structural and functional imaging, to provide a more comprehensive understanding of epileptogenic network alterations in epilepsy.

CONCLUSIONS

The fusion of FDG and FMZ PET, in conjunction with machine learning techniques, represents a novel and powerful tool for detecting and characterizing the epileptogenic zone in TLE patients. This approach has potential implications for improving surgical planning and predicting surgical outcomes, thereby contributing to optimizing patient management in epilepsy care.

ACKNOWLEDGMENTS

This project partially supported by the National Natural Science Foundation of China projects 82272116 and 62101321, and the Science and Technology Commission of Shanghai municipality frontier innovation program 24DP3200600.

REFERENCES

1. Beghi E. The Epidemiology of Epilepsy. *Neuroepidemiology.* 2020;54(2):185-191.
2. Zijlmans M, Zweiphenning W, van Klink N. Changing concepts in presurgical assessment for epilepsy surgery. *Nat Rev Neurol.* 2019;15(10):594-606.
3. Bartolomei F, Chauvel P, Wendling F. Epileptogenicity of brain structures in human temporal lobe epilepsy: a quantified study from intracerebral EEG. *Brain.* 2008;131(Pt 7):1818-1830.
4. Mullin JP, Shriver M, Alomar S, et al. Is SEEG safe? A systematic review and meta-analysis of stereo-electroencephalography-related complications. *Epilepsia.* 2016;57(3):386-401.
5. Lamusuo S, Jutila L, Ylinen A, et al. [18F]FDG-PET reveals temporal hypometabolism in patients with temporal lobe epilepsy even when quantitative MRI and histopathological analysis show only mild hippocampal damage. *Arch Neurol.* 2001;58(6):933-939.

6. Traub-Weidinger T, Arbizu J, Barthel H, et al. EANM practice guidelines for an appropriate use of PET and SPECT for patients with epilepsy. *Eur J Nucl Med Mol Imaging.* 2024;51(7):1891-1908.
7. Chassoux F, Artiges E, Semah F, et al. Determinants of brain metabolism changes in mesial temporal lobe epilepsy. *Epilepsia.* 2016;57(6):907-919.
8. Zhang M, Huang H, Liu W, et al. Combined quantitative T2 mapping and [(18)F]FDG PET could improve lateralization of mesial temporal lobe epilepsy. *Eur Radiol.* 2022;32(9):6108-6117.
9. Huang H, Zhang M, Zhao Y, et al. Simultaneous high-resolution whole-brain MR spectroscopy and [18F]FDG PET for temporal lobe epilepsy. *Eur J Nucl Med Mol Imaging.* 2024;51(3):721-733.
10. Chassoux F, Rodrigo S, Semah F, et al. FDG-PET improves surgical outcome in negative MRI Taylor-type focal cortical dysplasias. *Neurology.* 2010;75(24):2168-2175.
11. Lagarde S, Boucekine M, McGonigal A, et al. Relationship between PET metabolism and SEEG epileptogenicity in focal lesional epilepsy. *Eur J Nucl Med Mol Imaging.* 2020;47(13):3130-3142.
12. Ryvlin P, Bouvard S, Le Bars D, et al. Clinical utility of flumazenil-PET versus [18F]fluorodeoxyglucose-PET and MRI in refractory partial epilepsy. A prospective study in 100 patients. *Brain.* 1998;121(11):2067-2081.
13. Vivash L, Gregoire MC, Lau EW, et al. 18F-flumazenil: a γ-aminobutyric acid A-specific PET radiotracer for the localization of drug-resistant temporal lobe epilepsy. *J Nucl Med.* 2013;54(8):1270-1277.
14. Jansen LA, Peugh LD, Roden WH, et al. Impaired maturation of cortical GABAA receptor expression in pediatric epilepsy. *Epilepsia.* 2010;51(8):1456-1467.
15. Deeb TZ, Maguire J, Moss SJ. Possible alterations in GABAA receptor signaling that underlie benzodiazepine-resistant seizures. *Epilepsia.* 2012;53 Suppl 9(0 9):79-88.
16. Alhourani A, Fish KN, Wozny TA, et al. GABA bouton subpopulations in the human dentate gyrus are differentially altered in mesial temporal lobe epilepsy. *J Neurophysiol.* 2020;123(1):392-406.
17. Benarroch EE. GABAA receptor heterogeneity, function, and implications for epilepsy. *Neurology.* 2007;68(8):612-614.
18. Niu N, Xing H, Wu M, et al. Performance of PET imaging for the localization of epileptogenic zone in patients with epilepsy: a meta-analysis. *Eur Radiol.* 2021;31(8):6353-6366.
19. Hodolic M, Topakian R, Pichler R. (18)F-fluorodeoxyglucose and (18)F-flumazenil positron emission tomography in patients with refractory epilepsy. *Radiol Oncol.* 2016;50(3):247-253.
20. Avendaño-Estrada A, Velasco F, Velasco Ana L, et al. Quantitative Analysis of [18F]FFMZ and [18F]FDG PET Studies in the Localization of Seizure Onset Zone in Drug-Resistant Temporal Lobe Epilepsy. *Stereotact Funct Neurosurg.* 2019;97(4):232-240.
21. Li G, Jiang S, Chen C, et al. iEEGview: an open-source multifunction GUI-based Matlab toolbox for localization and visualization of human intracranial electrodes. *J Neural Eng.* 2019;17(1):016016.
22. Destrieux C, Fischl B, Dale A, et al. Automatic parcellation of human cortical gyri and sulci using standard anatomical nomenclature. *Neuroimage.* 2010;53(1):1-15.
23. Mercier MR, Dubarry AS, Tadel F, et al. Advances in human intracranial electroencephalography research, guidelines and good practices. *Neuroimage.* 2022;260:119438.
24. Lagarde S, Roehri N, Lambert I, et al. Interictal stereotactic-EEG functional connectivity in refractory focal epilepsies. *Brain.* 2018;141(10):2966-2980.
25. Ryzhikov NN, Seneca N, Krasikova RN, et al. Preparation of highly specific radioactivity [18F]flumazenil and its evaluation in cynomolgus monkey by positron emission tomography. *Nucl Med Biol.* 2005;32(2):109-116.
26. Radua J, Vieta E, Shinohara R, et al. Increased power by harmonizing structural MRI site differences with the ComBat batch adjustment method in ENIGMA. *Neuroimage.* 2020;218:116956.
27. Rizzo S, Botta F, Raimondi S, et al. Radiomics: the facts and the challenges of image analysis. *Eur Radiol Exp.* 2018;2(1):36.
28. Garofalo S, Giovagnoli S, Orsoni M, et al. Interaction effect: Are you doing the right thing? *PLoS One.* 2022;17(7):e0271668.
29. Iacobucci D, Schneider MJ, Popovich DL, et al. Mean centering helps alleviate "micro" but not "macro" multicollinearity. *Behavior Research Methods.* 2016;48(4):1308-1317.
30. Tibshirani R. Regression Shrinkage and Selection Via the Lasso. *Journal of the Royal Statistical Society: Series B (Methodological).* 1996;58(1):267-288.
31. Laschet JJ, Kurcewicz I, Minier F, et al. Dysfunction of GABAA receptor glycolysis-dependent modulation in human partial epilepsy. *Proc Natl Acad Sci U S A.* 2007;104(9):3472-3477.
32. Holthoff VA, Koeppe RA, Frey KA, et al. Positron emission tomography measures of benzodiazepine receptors in Huntington's disease. *Annals of Neurology.* 1993;34(1):76-81.
33. Nedergaard S, Andreasen M. Opposing effects of 2-deoxy-d-glucose on interictal- and ictal-like activity when K(+) currents and GABA(A) receptors are blocked in rat hippocampus in vitro. *J Neurophysiol.* 2018;119(5):1912-1923.
34. Kim K, Yoon H. Gamma-Aminobutyric Acid Signaling in Damage Response, Metabolism, and Disease. *Int J Mol Sci.* 2023;24(5).
35. Nørgaard M, Beliveau V, Ganz M, et al. A high-resolution in vivo atlas of the human brain's benzodiazepine binding site of GABA(A) receptors. *Neuroimage.* 2021;232:117878.

SUPPLEMENTAL FILES

Summary of the supplementary file

Table S1. STARD 2015 checklist

Section & Topic	No	Item	Reported on page#
TITLE OR ABSTRACT			
	1	Identification as a study of diagnostic accuracy using at least one measure of accuracy (such as sensitivity, specificity, predictive values, or AUC)	Page 1
ABSTRACT			
	2	Structured summary of study design, methods, results, and conclusions (for specific guidance, see STARD for Abstracts)	Page 1
INTRODUCTION			
	3	Scientific and clinical background, including the intended use and clinical role of the index test	Page 2
	4	Study objectives and hypotheses	Page 2
METHODS			
Study design	**5**	Whether data collection was planned before the index test and reference standard were performed (prospective study) or after (retrospective study)	Page 2
Participants	**6**	Eligibility criteria	Page 2
	7	On what basis potentially eligible participants were identified (such as symptoms, results from previous tests, inclusion in registry)	Page 2
	8	Where and when potentially eligible participants were identified (setting, location and dates)	Page 2
	9	Whether participants formed a consecutive, random or convenience series	Page 2
Test methods	**10a**	Index test, in sufficient detail to allow replication	Page 2 – 4
	10b	Reference standard, in sufficient detail to allow replication	Page 2 – 4
	11	Rationale for choosing the reference standard (if alternatives exist)	Page 2 – 4
	12a	Definition of and rationale for test positivity cut-offs or result categories of the index test, distinguishing pre-specified from exploratory	Page 4
	12b	Definition of and rationale for test positivity cut-offs or result categories of the reference standard, distinguishing pre-specified from exploratory	Page 4
	13a	Whether clinical information and reference standard results were available to the performers/readers of the index test	Page 2
	13b	Whether clinical information and index test results were available to the assessors of the reference standard	Page 2
Analysis	**14**	Methods for estimating or comparing measures of diagnostic accuracy	Page 4
	15	How indeterminate index test or reference standard results were handled	Page 4
	16	How missing data on the index test and reference standard were handled	Page 4
	17	Any analyses of variability in diagnostic accuracy, distinguishing pre-specified from exploratory	Page 2-4
	18	Intended sample size and how it was determined	Page 2
RESULTS			
Participants	**19**	Flow of participants, using a diagram	Page 3
	20	Baseline demographic and clinical characteristics of participants	Page 4
	21a	Distribution of severity of disease in those with the target condition	Page 4 - 6
	21b	Distribution of alternative diagnoses in those without the target condition	Page 4 – 6
	22	Time interval and any clinical interventions between index test and reference standard	Page 2
Test results	**23**	Cross tabulation of the index test results (or their distribution) by the results of the reference standard	-

	24	Estimates of diagnostic accuracy and their precision (such as 95% confidence intervals)	Page 6 - 7
	25	Any adverse events from performing the index test or the reference standard	-
DISCUSSION			
	26	Study limitations, including sources of potential bias, statistical uncertainty, and generalisability	Page 8
	27	Implications for practice, including the intended use and clinical role of the index test	Page 8
OTHER INFORMATION			
	28	Registration number and name of registry	Page 2
	29	Where the full study protocol can be accessed	Page 2 – 4
	30	Sources of funding and other support; role of funders	Page 1

Table S2. Detailed patient demographic and clinical information*

Patient ID	*Age*	*Sex*	*Age of onset (year)*	*Epilepsy duration (year)*	*Seizure frequency*	*MRI diagnosis*	*EZ location*	*Engel class (>1 year)*
1	42	F	40	2	3-4/day	B	R HIP	I
2	29	F	5	24	7-8/month	P	L HIP	I
3	15	M	13	2	3/year	B	L HIP	I
4	21	F	14	7	1-2/year	B	L HIP	I
5	38	F	16	22	1/week	B	R HIP	I
6	32	M	27	5	6/year	B	R HIP	I
7	24	F	17	7	2-3/month	B	R HIP	I
8	29	M	9	20	2-3/month	B	R HIP	I
9	34	F	25	9	2-3/month	B	L HIP	I
10	32	M	27	5	3-4/week	P	L HIP	I
11	32	M	15	17	2-3/month	B	R HIP	II
12	27	M	1	26	4-5/month	B	R HIP	I
13	46	F	34	12	2-8/month	N	L HIP	I
14	32	M	16	15	2-3/month	B	R HIP	I
15	41	F	34	8	2/year	N	L TPO	I
16	52	F	20	32	1-2/month	P	R TPO	I
17	33	M	22	11	1-2/day	P	R ITG	I
18	33	M	23	10	2-3/week	P	L ITG	I
19	19	M	12	7	2-3/month	P	R TPO	I
20	8	M	4	4	1/month	N	L STG	I

Note: *all subjects had an interval of more than 24 hours to ensure decay of the radioisotope and less than 1 year between the two scans. B, bilateral abnormalities, indicates inconclusive findings on MRI; F, female; L HIP, left hippocampus; L ITG, left inferior temporal gyrus; L STG, superior temporal gyrus; L TPO: left temporal pole; M, male; N, cases with MRI-negative findings; P, cases with MRI-positive findings that are distinctly lateralized; R HIP: right hippocampus; R ITG, right inferior temporal gyrus; R TPO: right temporal pole.

Table S3. Performance evaluations of epileptogenic zone prediction in all patients

	EZ vs. NIZ				EZ vs. PZ				PZ vs. NIZ			
Parameters	AUC	Acc	Sen	Spe	AUC	Acc	Sen	Spe	AUC	Acc	Sen	Spe
FDG	0.80	0.78	0.67	0.81	0.74	0.74	0.63	0.77	0.59	0.59	0.52	0.67
FMZ	0.78	0.74	0.68	0.76	0.72	0.65	0.74	0.63	0.57	0.57	0.40	0.74
FDG+FMZ	0.82	0.77	0.78	0.77	0.77	0.72	0.73	0.72	0.61	0.60	0.66	0.54
FDG+FMZ+Fusion	0.86	0.82	0.76	0.84	0.79	0.74	0.71	0.75	0.62	0.60	0.59	0.62

Note: AUC, the area under the curve; ACC, accuracy; EZ, epileptogenic zone; NIZ non-involved zone; PZ, propagation zone; Sen, sensitivity; Spe, specificity.

Table S4. Performance evaluations of epileptogenic zone prediction in mesial TLE patients

	EZ vs. NIZ				EZ vs. PZ				PZ vs. NIZ			
Parameters	AUC	Acc	Sen	Spe	AUC	Acc	Sen	Spe	AUC	Acc	Sen	Spe
FDG	0.85	0.81	0.71	0.83	0.79	0.75	0.68	0.76	0.62	0.61	0.53	0.70
FMZ	0.81	0.76	0.73	0.77	0.77	0.68	0.77	0.66	0.57	0.57	0.39	0.75
FDG+FMZ	0.87	0.82	0.81	0.82	0.81	0.74	0.78	0.74	0.63	0.62	0.69	0.55
FDG+FMZ+Fusion	0.89	0.86	0.79	0.87	0.83	0.77	0.77	0.77	0.64	0.62	0.61	0.64

Note: AUC, the area under the curve; ACC, accuracy; EZ, epileptogenic zone; NIZ non-involved zone; PZ, propagation zone; Sen, sensitivity; Spe, specificity.

Table S5. Performance evaluations of epileptogenic zone prediction in lateral TLE patients

	EZ vs. NIZ				EZ vs. PZ				PZ vs. NIZ			
Parameters	AUC	Acc	Sen	Spe	AUC	Acc	Sen	Spe	AUC	Acc	Sen	Spe
FDG	0.66	0.71	0.56	0.75	0.62	0.72	0.50	0.80	0.52	0.52	0.47	0.57
FMZ	0.68	0.70	0.57	0.74	0.59	0.58	0.66	0.55	0.56	0.57	0.42	0.71
FDG+FMZ	0.69	0.66	0.70	0.64	0.65	0.64	0.62	0.65	0.55	0.53	0.57	0.49
FDG+FMZ+Fusion	0.76	0.72	0.70	0.73	0.67	0.67	0.58	0.70	0.55	0.54	0.53	0.55

Note: AUC, the area under the curve; ACC, accuracy; EZ, epileptogenic zone; NIZ non-involved zone; PZ, propagation zone; Sen, sensitivity; Spe, specificity.

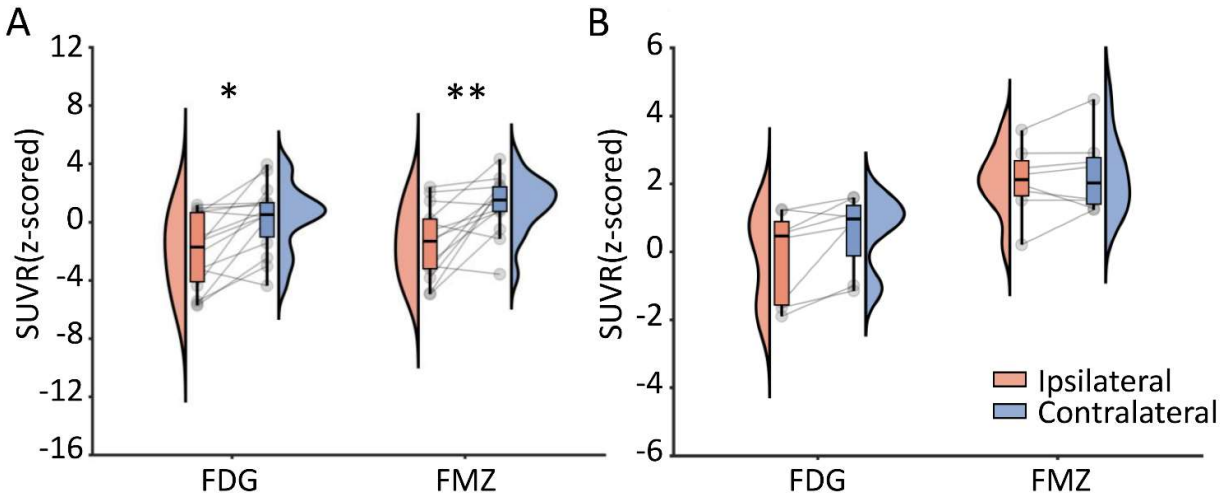

Figure S1. Comparison of ipsilateral vs. contralateral FDG and FMZ SUVR in the hippocampus of (A) mesial TLE patients and (B) lateral TLE patients.

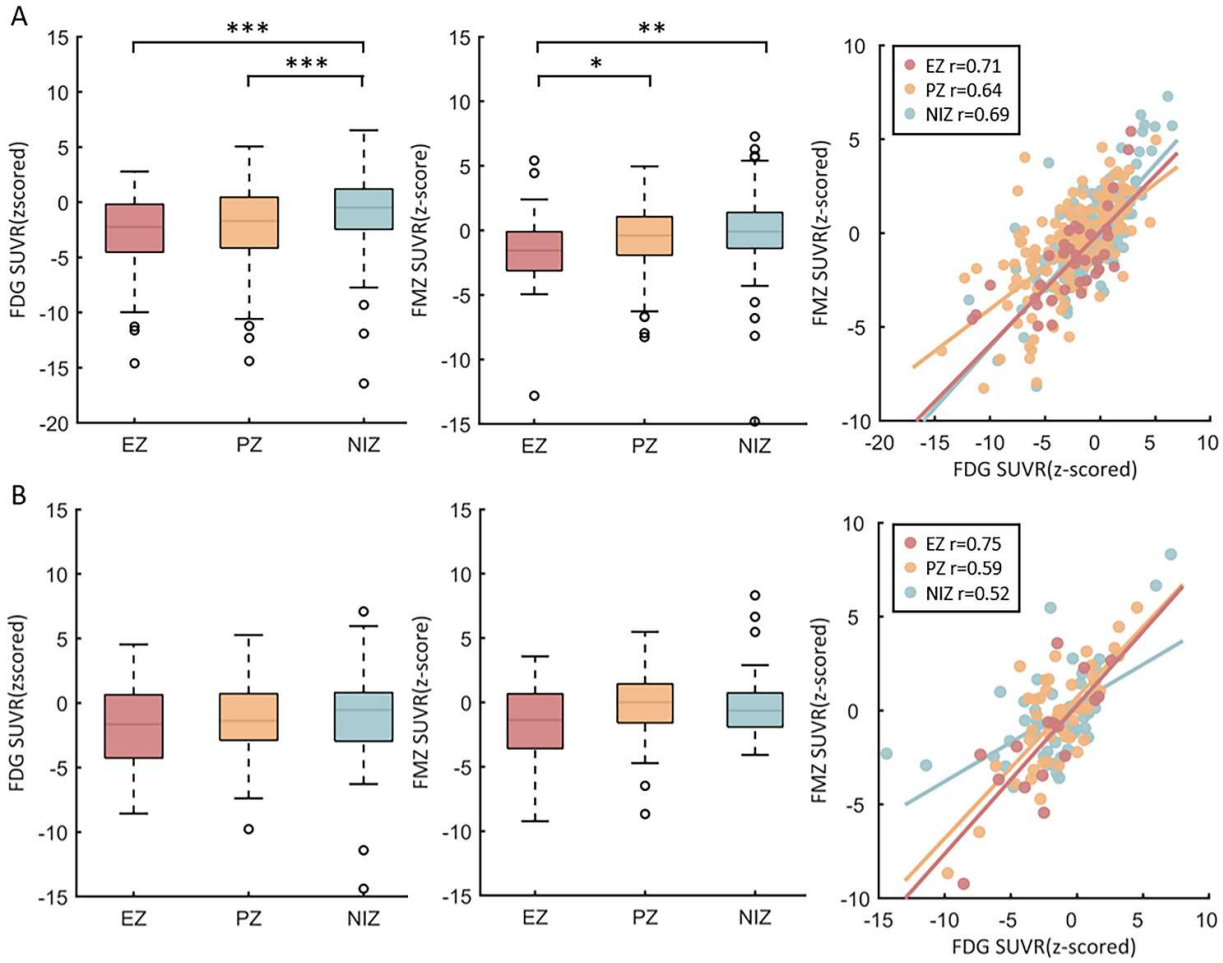

Figure S2. Comparisons of FDG and FMZ SUVR among brain regions with different epileptogenicity in patients with (A) mesial TLE and (B) lateral TLE. ***P < .001, Mann-Whitney U test under Bonferroni-Holm correction.

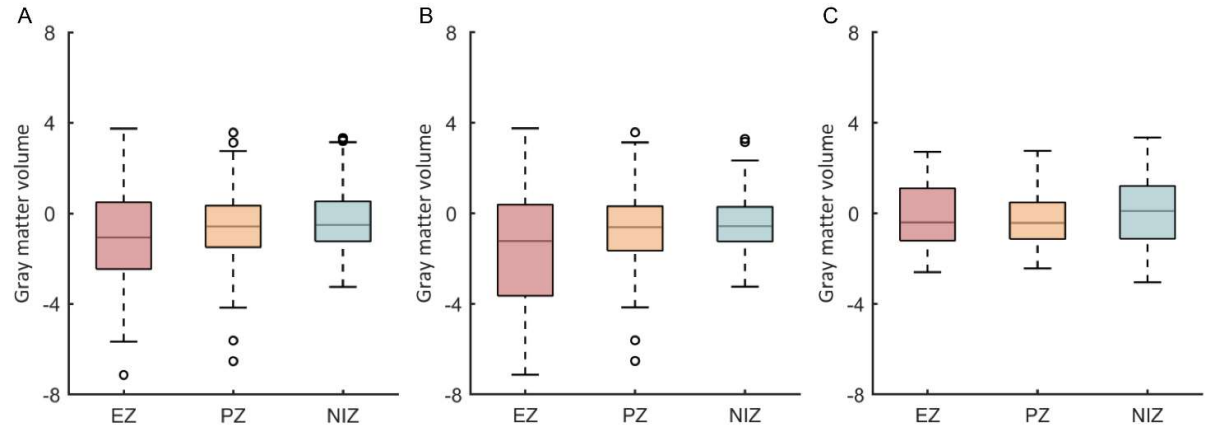

Figure S3. Comparisons of gray matter volume in regions with different epileptogenicity of different subgroups: (A) all patients, (B) mesial TLE patients, and (C) lateral TLE patients. Mann-Whitney U test under Bonferroni-Holm correction.

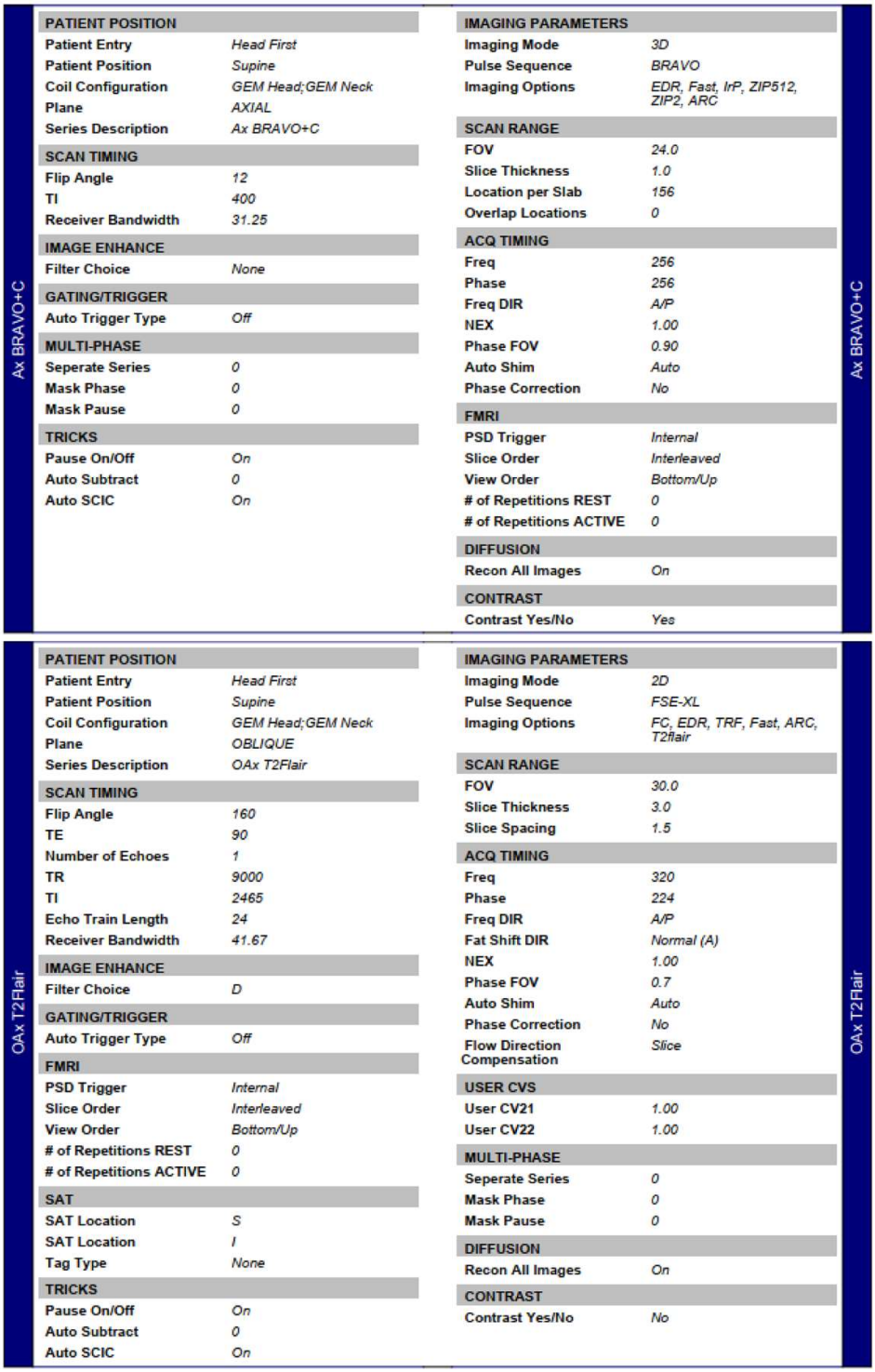

Ax BRAVO+C

PATIENT POSITION	
Patient Entry	Head First
Patient Position	Supine
Coil Configuration	GEM Head;GEM Neck
Plane	AXIAL
Series Description	Ax BRAVO+C
SCAN TIMING	
Flip Angle	12
TI	400
Receiver Bandwidth	31.25
IMAGE ENHANCE	
Filter Choice	None
GATING/TRIGGER	
Auto Trigger Type	Off
MULTI-PHASE	
Seperate Series	0
Mask Phase	0
Mask Pause	0
TRICKS	
Pause On/Off	On
Auto Subtract	0
Auto SCIC	On

IMAGING PARAMETERS	
Imaging Mode	3D
Pulse Sequence	BRAVO
Imaging Options	EDR, Fast, IrP, ZIP512, ZIP2, ARC
SCAN RANGE	
FOV	24.0
Slice Thickness	1.0
Location per Slab	156
Overlap Locations	0
ACQ TIMING	
Freq	256
Phase	256
Freq DIR	A/P
NEX	1.00
Phase FOV	0.90
Auto Shim	Auto
Phase Correction	No
FMRI	
PSD Trigger	Internal
Slice Order	Interleaved
View Order	Bottom/Up
# of Repetitions REST	0
# of Repetitions ACTIVE	0
DIFFUSION	
Recon All Images	On
CONTRAST	
Contrast Yes/No	Yes

Ax BRAVO+C

OAx T2Flair

PATIENT POSITION	
Patient Entry	Head First
Patient Position	Supine
Coil Configuration	GEM Head;GEM Neck
Plane	OBLIQUE
Series Description	OAx T2Flair
SCAN TIMING	
Flip Angle	160
TE	90
Number of Echoes	1
TR	9000
TI	2465
Echo Train Length	24
Receiver Bandwidth	41.67
IMAGE ENHANCE	
Filter Choice	D
GATING/TRIGGER	
Auto Trigger Type	Off
FMRI	
PSD Trigger	Internal
Slice Order	Interleaved
View Order	Bottom/Up
# of Repetitions REST	0
# of Repetitions ACTIVE	0
SAT	
SAT Location	S
SAT Location	I
Tag Type	None
TRICKS	
Pause On/Off	On
Auto Subtract	0
Auto SCIC	On

IMAGING PARAMETERS	
Imaging Mode	2D
Pulse Sequence	FSE-XL
Imaging Options	FC, EDR, TRF, Fast, ARC, T2flair
SCAN RANGE	
FOV	30.0
Slice Thickness	3.0
Slice Spacing	1.5
ACQ TIMING	
Freq	320
Phase	224
Freq DIR	A/P
Fat Shift DIR	Normal (A)
NEX	1.00
Phase FOV	0.7
Auto Shim	Auto
Phase Correction	No
Flow Direction Compensation	Slice
USER CVS	
User CV21	1.00
User CV22	1.00
MULTI-PHASE	
Seperate Series	0
Mask Phase	0
Mask Pause	0
DIFFUSION	
Recon All Images	On
CONTRAST	
Contrast Yes/No	No

OAx T2Flair

Figure S4. The MR imaging protocols.